EMBRY-RIDDLE Aeronautical University
SCHOLARLY COMMONS

Publications

1-2006

The White Dwarf Luminosity Function from Sloan Digital Sky Survey Imaging Data

Hugh C. Harris
US Naval Observatory, hch@nofs.navy.mil

Jeffrey A. Munn
US Naval Observatory, jam@nofs.navy.mil

Mukremin Kilic
University of Texas at Austin, kilic@ou.edu

James W. Liebert
University of Arizona, Steward Observatory, jamesliebert@gmail.com

Kurtis A. Williams
University of Arizona, Steward Observatory

See next page for additional authors

Follow this and additional works at: https://commons.erau.edu/publication

Part of the Stars, Interstellar Medium and the Galaxy Commons

Scholarly Commons Citation

Harris, H. C., Munn, J. A., Kilic, M., Liebert, J. W., Williams, K. A., von Hippel, T., Levine, S. E., Monet, D. G., Eisenstein, D. J., Kleinman, S. J., Metcalfe, T. S., Nikka, A., Winget, D. E., Brinkmann, J., Fukugita, M., Knapp, G. R., Lupton, R. H., Smith, J. A., & Schneider, D. P. (2006). The White Dwarf Luminosity Function from Sloan Digital Sky Survey Imaging Data. *The Astronomical Journal, 131*(1). Retrieved from https://commons.erau.edu/publication/219

This Article is brought to you for free and open access by Scholarly Commons. It has been accepted for inclusion in Publications by an authorized administrator of Scholarly Commons. For more information, please contact commons@erau.edu, wolfe309@erau.edu.

Authors
Hugh C. Harris, Jeffrey A. Munn, Mukremin Kilic, James W. Liebert, Kurtis A. Williams, Ted von Hippel, Stephen E. Levine, David G. Monet, Daniel J. Eisenstein, S. J. Kleinman, T. S. Metcalfe, Atsuko Nikka, D. E. Winget, J. Brinkmann, Masataka Fukugita, G. R. Knapp, Robert H. Lupton, J. Allyn Smith, and Donald P. Schneider

This article is available at Scholarly Commons: https://commons.erau.edu/publication/219

The Astronomical Journal, 131:571–581, 2006 January
© 2006. The American Astronomical Society. All rights reserved. Printed in U.S.A.

THE WHITE DWARF LUMINOSITY FUNCTION FROM SLOAN DIGITAL SKY SURVEY IMAGING DATA

Hugh C. Harris,[1] Jeffrey A. Munn,[1] Mukremin Kilic,[2] James Liebert,[3] Kurtis A. Williams,[3] Ted von Hippel,[2] Stephen E. Levine,[1] David G. Monet,[1] Daniel J. Eisenstein,[3] S. J. Kleinman,[4] T. S. Metcalfe,[5] Atsuko Nitta,[4] D. E. Winget,[2] J. Brinkmann,[4] Masataka Fukugita,[6] G. R. Knapp,[7] Robert H. Lupton,[7] J. Allyn Smith,[8,9] and Donald P. Schneider[10]
Received 2005 March 19; accepted 2005 September 9

ABSTRACT

A sample of white dwarfs is selected from the Sloan Digital Sky Survey (SDSS) Data Release 3 using their reduced proper motions, based on improved proper motions from combined SDSS and USNO-B data. Numerous SDSS and follow-up spectra (Kilic and coworkers) are used to quantify completeness and contamination of the sample; kinematics models are used to understand and correct for velocity-dependent selection biases. A luminosity function is constructed covering the range $7 < M_{\rm bol} < 16$, and its sensitivity to various assumptions and selection limits is discussed. The white dwarf luminosity function based on 6000 stars is remarkably smooth and rises nearly monotonically to $M_{\rm bol} = 15.3$. It then drops abruptly, although the small number of low-luminosity stars in the sample and their unknown atmospheric composition prevent quantitative conclusions about this decline. Stars are identified that may have high tangential velocities, and a preliminary luminosity function is constructed for them.

Key words: astrometry — solar neighborhood — stars: kinematics — stars: luminosity function, mass function — white dwarfs

1. INTRODUCTION

The white dwarf luminosity function (WDLF) is important in providing a record of the star formation history and the age of each of the components of the Galaxy in the solar neighborhood. Historically, the hot end of the WDLF has been determined by a selection of blue stars (e.g., Fleming et al. 1986; Vennes et al. 2002; Liebert et al. 2005), while the WDLF at medium and cool WD temperatures often has been determined by a selection that includes proper motion (e.g., Liebert et al. 1988; Boyle 1989; Evans 1992; Oswalt et al. 1996; Knox et al. 1999). The faintness and rarity of WDs requires that large areas of the sky be covered in order to acquire a large WD sample and to determine the WDLF accurately. Photographic survey data generally provide poor-quality photometry that hampers WD selection. The desirable goals of high-accuracy photometry and astrometry over wide areas of the sky motivate us to use digital surveys such as the Sloan Digital Sky Survey (SDSS).

The SDSS (York et al. 2000; Stoughton et al. 2002; Gunn et al. 1998) obtains images of the sky in a survey area around the north Galactic cap and in other smaller areas. From these images, calibrated photometry in the five *ugriz* filters (Fukugita et al. 1996; Lupton et al. 2001; Hogg et al. 2001; Smith et al. 2002; Ivezíc et al. 2004) and star-galaxy image classification are obtained for all detected objects. The SDSS then obtains spectra of many objects, primarily galaxies and QSOs and a small fraction of stars. For purposes of studying WDs, spectra are obtained of essentially all hot WDs with $T > 22{,}000$ K and of many medium-temperature WDs with 8000 K $< T <$ 22,000 K (Harris et al. 2003; Kleinman et al. 2004), but of very few cool WDs with 4000 K $< T <$ 8000 K, until they reach the rare ultracool temperatures $T < 4000$ K (Gates et al. 2004). This incomplete sampling of the spectra of WDs with cool and intermediate temperatures, just in the temperature range in which the LF is near its maximum, is a result of their colors overlapping the far more numerous F, G, and K main-sequence stars. An attempt to distinguish cool WDs from field stars by combining SDSS photometry with another narrowband magnitude was only partially successful (Kilic et al. 2004). Therefore, neither spectroscopic nor photometric selection of WDs in the SDSS are useful approaches for studying the WDLF at intermediate and cool temperatures.

Instead, identification of WDs with cool and intermediate temperatures in SDSS imaging data is feasible by including proper motions. This paper uses proper motions derived from combined SDSS and USNO-B astrometry, along with SDSS photometry, to define a sample of WDs selected using reduced proper motions (RPMs). The WDLF based on this sample is presented, and the important factors and limitations of the data are discussed. The selection procedure is described in § 2. Factors that should be accounted for in constructing the WDLF are discussed in § 3, including estimates of the completeness and contamination of the WD selection. In § 4 initial results are presented for the WDLF based on SDSS Data Release 3 (DR3; Abazajian et al. 2005).

2. SELECTION OF WHITE DWARFS BY REDUCED PROPER MOTION

Identification of WDs in SDSS imaging data is done here using the RPM diagram. The RPM, in g magnitude, for example, is defined as

$$H_g = g + 5\log\mu + 5 = M_g + 5\log V_{\rm tan} - 3.379,$$

[1] US Naval Observatory, 10391 West Naval Observatory Road, Flagstaff, AZ 86001-8521; hch@nofs.navy.mil.
[2] Department of Astronomy, University of Texas at Austin, 1 University Station C1400, Austin, TX 78712.
[3] Steward Observatory, University of Arizona, 933 North Cherry Avenue, Tucson, AZ 85721.
[4] Apache Point Observatory, P.O. Box 59, Sunspot, NM 88349-0059.
[5] Harvard-Smithsonian Center for Astrophysics, Mail Stop 16, 60 Garden Street, Cambridge, MA 02138.
[6] Institute for Cosmic Ray Research, University of Tokyo, 5-1-5 Kashiwa, Kashiwa City, Chiba 277-8582, Japan.
[7] Princeton University Observatory, Peyton Hall, Princeton, NJ 08544.
[8] Los Alamos National Laboratory, P.O. Box 1663, Los Alamos, NM 87545.
[9] Department of Physics and Astronomy, University of Wyoming, P.O. Box 3905, Laramie, WY 82071.
[10] Department of Astronomy and Astrophysics, Pennsylvania State University, 525 Davey Laboratory, University Park, PA 16802.

where μ is the proper motion in arcseconds per year and $V_{\rm tan}$ is the tangential velocity in kilometers per second. The RPM provides a distance-independent tool for separating stars with very different absolute magnitudes. WDs are typically 5–7 mag less luminous than subdwarfs of the same color, so they have RPM values typically 3–4 mag fainter than subdwarfs after the approximately 3 times greater velocity dispersion of subdwarfs is accounted for. The RPM diagram has been used in previous studies to identify WDs (Evans 1992; Knox et al. 1999; Oppenheimer et al. 2001; Nelson et al. 2002) and subdwarfs (e.g., Digby et al. 2003). The accurate SDSS colors help in the separation of different stellar populations.

Calculating values of RPM requires measuring proper motions, and SDSS is, in general, only a single-epoch survey. However, matching SDSS objects with a catalog made from sky survey plates immediately makes it possible to measure the proper motions for most objects bright enough to be detected and included in the plate-based catalog. This paper uses the improved proper motion catalog given by Munn et al. (2004), extended to include the area of 5282 deg^2 of sky in the SDSS DR3 (Abazajian et al. 2005). It is based on matches to the all-sky USNO-B Catalog (Monet et al. 2003), but it includes proper motions that are improved over those in USNO-B both by including the SDSS positions (Pier et al. 2003) and by correcting the sky survey positions to an inertial system using galaxies; see Munn et al. (2004) for details. The minimum proper motion of 20 mas yr^{-1} used by Munn et al. is also used here, eliminating nearly all QSOs and many nondegenerate stars. The resulting catalog has errors in proper motion of 3–4 mas yr^{-1} and is nearly 90% complete at $g = 19.5$; we discuss the effects of these errors and incompleteness in § 3.4.

In a companion paper, Kilic et al. (2006) present the RPM diagram (their Figs. 1 and 6) based on the Munn et al. (2004) catalog. Kilic et al. use SDSS spectroscopy, as well as follow-up spectroscopy of regions of the RPM diagram expected to be occupied by cool WDs but not observed spectroscopically by SDSS; they confirm that WDs occupy a locus in the RPM diagram cleanly separated from most subdwarfs and that samples of WDs can be defined using the RPM diagram with contamination by subdwarfs and QSOs of only a few percent. We use that result to create statistically complete catalogs of WDs. A region of the RPM diagram is defined by a curve showing the cooling track of WDs with pure hydrogen atmospheres, using the models of Bergeron et al. (1995), for some assumed tangential velocity. A sample of WDs is defined by taking all stars below and blueward of one of the model curves (for example, the $V_{\rm tan} = 30$ km s^{-1} curve for pure hydrogen atmosphere WDs). Using $V_{\rm tan}$ cutoffs of 20, 30, and 40 km s^{-1} yields samples of 7116, 6000, and 4501 stars, respectively. The extent of contamination and incompleteness, the procedure used to correct for interstellar reddening, and other issues relevant to the LF calculation are discussed in § 3. The list of stars selected with $V_{\rm tan} > 20$ km s^{-1} is given in a file available by anonymous FTP.[11]

3. CONSTRUCTION OF THE LUMINOSITY FUNCTION

The LF is calculated based on distances to each star derived from photometry (see §§ 3.1 and 3.2). The high-quality SDSS photometry greatly aids this procedure. The effects of the disk scale height and completeness are discussed in §§ 3.3 and 3.4. In § 3.5 we examine and apply corrections for contamination. The problem of accounting for the different properties of hydrogen and helium atmospheres of cool WDs is discussed in § 3.6.

3.1. *WD + M Binaries*

Some WD candidates have unresolved dM companions (Raymond et al. 2003; Kleinman et al. 2004; Smolcić et al. 2004). They are identified in this paper in the following way: When all five SDSS magnitudes are fitted to WD model colors, stars that have a (poor) best fit with $\chi^2 > 20$ and that have significant excess residual u and z flux from the best-fit model are designated as having a significant cool companion. (The dM companion contributes to the red filters, but the initial fit tries to match the composite flux distribution, so the compromise WD model is too cool and residual excess flux is observed in both u and z filters.) These stars are shown as filled circles in Figure 1. About 2.5% of the sample selected by proper motion in this paper are found in this way to be composite. For these stars, the remaining analysis is carried out using only the *ugr* magnitudes to fit the temperature, luminosity, distance, etc. Omitting the i and z magnitudes minimizes the effect of the cool companions but does not entirely eliminate it. In practice, those WDs with fainter cool companions are analyzed approximately correctly with this procedure, a few WDs with companions of similar brightness at i have their luminosities and distances underestimated, and WDs with bright companions are lost entirely from our sample.

3.2. *Photometric Distances*

All five SDSS magnitudes (three for the binaries in § 3.1) for each star are fitted to WD models with hydrogen atmospheres to determine the temperature, absolute magnitude, and distance of each star. The models of Bergeron et al. (1995) are used, with SDSS colors kindly calculated by P. Bergeron (2001, private communication), assuming $\log g = 8$, and accounting for reddening.[12] Approximate corrections from the observed SDSS u and z magnitudes onto the AB flux system of -0.04 and $+0.02$, respectively (Abazajian et al. 2004), are also included here. Colors of the Bergeron et al. (1995) models are plotted in Figure 2. They show that for warmer WDs the H/He composition has little effect, provided the gravity is normal. Incorrect luminosities and distances will be derived for WDs with unusually low mass and gravity, believed to be about 10% of all WDs (Bergeron et al. 1992; Liebert et al. 2005), and those with unusually high mass and gravity, believed to be about 15% of all WDs, as shown by the dotted curves displaced from the normal-gravity curves in Figure 2. The actual percentages of WDs with abnormal masses in our sample with magnitude and RPM limits will be somewhat different; the percentages are fairly small, and the effects are in opposite directions, so we ignore them here.

For warmer WDs with $T > 5500$ K ($g - i < 0.7$), the $M_{\rm bol}$ and M_g magnitudes of the pure hydrogen and pure helium

[11] See ftp://ftp.nofs.navy.mil/pub/outgoing/hch/tabdata.dat.

[12] The SDSS database gives the total interstellar absorption and reddening along the line of sight for each star, determined from the reddening maps of Schlegel et al. (1998). Because most of the WDs in this paper have distances within a few hundred parsecs, they are affected by only a fraction of the total absorption and reddening. This fraction is determined as part of the fitting for the distance of each star in an iterative procedure. We make the assumption that the absorption is zero for stars with distances <100 pc, that it is the full absorption for stars with distances from the Galactic plane $|z| > 250$ pc, and that the absorption varies linearly along the line of sight between these distances. Because all stars in this paper are at relatively high Galactic latitudes, the total (maximum) absorption and reddening is small; for WDs in our sample, the median total absorption A_g is 0.10, and the median total reddening $E(g - i)$ is 0.04. Therefore, the errors in the reddening using this procedure are tiny and have little effect on the derived distances.

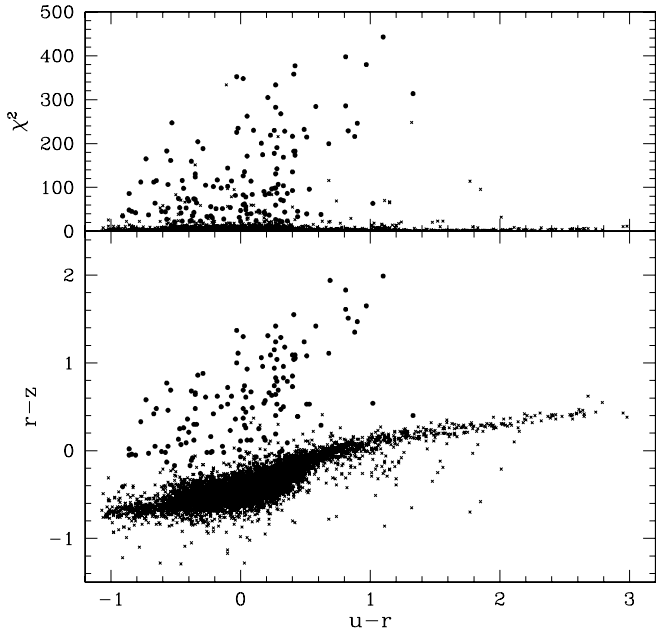

FIG. 1.—Identification of composite WDs with cool companions, shown by filled circles. *Top*: χ^2 values when all five SDSS magnitudes are fitted to model colors for WD candidates with $V_{\rm tan} > 30$ km s^{-1}. *Bottom*: Two-color diagram.

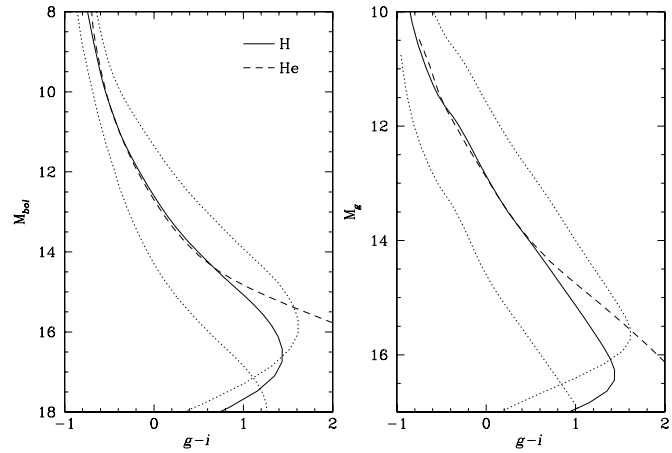

FIG. 2.—Color–absolute magnitude relations for model WDs with pure hydrogen (*solid line*) and pure helium (*dashed line*) atmospheres with $\log g = 8$ from Bergeron et al. (1995) models. Dotted lines show models with $\log g = 7$ for low-mass WDs (*upper line*) and $\log g = 9$ for high-mass WDs (*lower line*).

models versus $g - i$ in Figure 2 are nearly coincident. Therefore, the error in using pure hydrogen models for the minority of WDs that actually have helium atmospheres is expected to be small. Fitting the colors of a pure helium model with the grid of pure hydrogen models gives an error in $M_{\rm bol}$ that varies between +0.04 and −0.17 over the temperature range 5500–20,000 K. For example, a pure helium WD at 10,000 K has $M_{\rm bol} = 11.85$, but when fitted with a pure hydrogen model is assigned 10,090 K and $M_{\rm bol} = 11.78$. Thus, some will go into a luminosity bin higher than they should and be assigned a distance (and a $V_{\rm max}$ value) too small. The overall effect on the LF will be small. Of course, the few WDs with unusual abundances (DQ and DZ spectral types with strong absorption features) will have incorrect results, but these stars are a small fraction of the total (Harris et al. 2003; Kleinman et al. 2004).

For cool WDs with $T < 5500$ K ($g - i > 0.7$), the H/He composition does significantly affect the color–absolute magnitude relations in Figure 2 and the derived distance and luminosity. Independent data will be needed to utilize the SDSS sample fully. Deep infrared photometry might provide the needed H/He classification, for example. Lacking infrared data, we make a weighted H/He assignment for each cool star based on our knowledge of the fraction of each type from studies in the literature. We discuss the effects of this procedure in § 3.6.

Finally, of the seven published "ultracool" WDs with SDSS data (Gates et al. 2004; Harris et al. 1999, 2001), stars that are sufficiently cool that collision-induced absorption has a significant effect on their SDSS colors, three have $g < 19.5$ and can enter the sample. Photometric distance estimates cannot be relied on, however, because the WD models do not match the observed colors adequately (Gates et al. 2004, Fig. 1). Even worse, the distance is known only for LHS 3250, and that star is apparently undermassive and overluminous compared to the models that assume normal mass. Therefore, we adopt the same M_g and $M_{\rm bol}$ values for all three stars based on the trigonometric parallax of LHS 3250. (See Gates et al. for further discussion of this issue.) With this assumption, SDSS J0947 has $V_{\rm tan} =$ 19 km s^{-1} and drops out of the sample. LHS 3250 and SDSS J1403 are the only known ultracool WDs remaining in the sample. LHS 3250 has a known luminosity ($M_{\rm bol} = 16.2$); the assumption for the remainder of this paper is that SDSS J1403 has the same luminosity, although it is likely to be somewhat cooler and could have a lower luminosity (Gates et al. 2004). These two stars become the lowest luminosity WDs in the sample.

3.3. *Galactic Disk Scale Height*

The Galactic disk scale height of the WD population must be known before deriving the WDLF, because luminous WDs near the SDSS magnitude limit are at distances of several hundred parsecs from the Galactic plane, where their space density is significantly reduced. Normally, the scale height is determined by comparing the observed WD numbers versus $|z|$-distance to models of exponential disks with different assumed scale heights and finding the maximum likelihood fit. Some results from the literature are 245 ± 25 pc (Green 1980), ∼300 pc (Ishida et al. 1982), ∼270 pc (Downes 1986), 275 ± 50 pc (Boyle 1989), and 260 ± 40 pc (Vennes et al. 2002). Because these studies used relatively small WD samples (typically 100–200 stars), all stars were included in a single fit, and the models necessarily included an input LF to account for different numbers of stars at different luminosities. A consequence of this procedure is that the derived scale height and the derived LF are more coupled than is desirable.

SDSS provides a large enough sample to derive a scale height for *each* luminosity bin separately. Thus, the models to which the data are compared are each calculated for a single luminosity and require no assumptions about the LF. The models are constructed by taking the actual sky coverage of the survey area (for this paper, the imaging area covered by SDSS DR3) with its actual distribution of Galactic latitudes, taking the survey magnitude limits ($15.0 < g < 19.5$) and $V_{\rm tan}$ limit (30 km s^{-1}), and, for each luminosity bin, calculating the expected numbers of stars at each $|z|$-distance for different assumed values of scale height. A factor is also included to account for the exclusion of stars with small $V_{\rm tan}$ at large distances whose proper motions fall below the lower proper motion limit of 20 mas yr^{-1}.

Plots of the data for WDs in eight different luminosity ranges are shown in Figure 3, in which the data are fitted to models with scale heights of ∞, 500, 400, 300, and 200 pc (*top to bottom*). Table 1 shows the scale height and its uncertainty derived for each luminosity bin. The last three columns are the scale factor

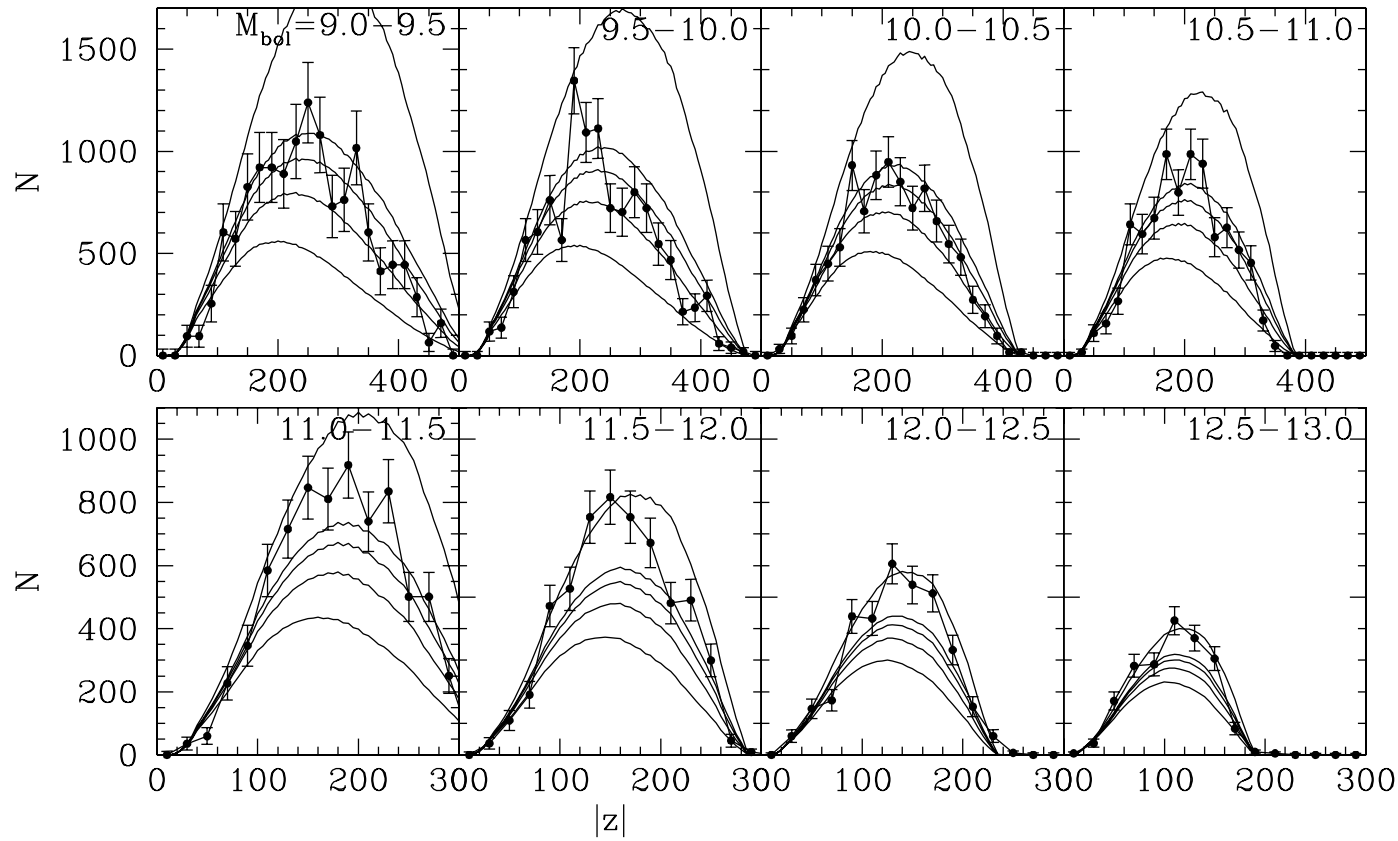

FIG. 3.—Distribution of WD candidates with distance from the Galactic plane for different luminosity bins. The curves in each panel show models of the distribution assuming disk scale heights of ∞, 500, 400, 300, and 200 pc (*top to bottom*).

needed to scale the observed number of stars to the best-fit model, the reduced χ^2 for the best-fit model, and the number of stars in the luminosity bin. It is unclear whether the trend shown in Table 1 of increasing scale height toward lower luminosity WDs is a result of some systematic effect in the selection or analysis of the WD sample or is real. A real increase in scale height is expected from the older age of the coolest WDs (coupled with the known heating of the Galactic disk with time), and possibly from an increasing fraction of thick-disk stars at cooler temperatures and lower luminosities. However, the large increase in Table 1 at $M_{\rm bol} \sim 12$ is probably not realistic (see § 5). Taking the first four bins ($9 < M_{\rm bol} < 11$), in which stars extend to large enough distances to be most sensitive to the scale height but thick-disk stars should still be a small minority, the weighted mean value of the scale height is 340^{+100}_{-70} pc. This result is somewhat larger than that of other studies in the literature, although consistent within the errors. More accurate results will come from analysis of hot WDs in the SDSS, in either a purely photometry-selected sample or a pure spectroscopic sample, in which the distances are greater and the requirement for proper motion selection can be dropped. Below we adopt 250 pc for the scale height for better comparison with those other studies. The effect on the WDLF of adopting different values is shown in § 4, and further discussion of the increasing scale height at low luminosities is in § 5.

TABLE 1
GALACTIC DISK SCALE HEIGHT

$M_{\rm bol}$	Scale Height (pc) Value	Minimum	Maximum	SF	χ^2_ν	N
9.0–9.5	326	185	780	127.3	1.48	424
9.5–10.0	319	185	700	78.1	1.98	586
10.0–10.5	355	195	∞	64.2	0.73	613
10.5–11.0	354	190	∞	62.6	2.54	547
11.0–11.5	463	240	∞	47.7	2.69	627
11.5–12.0	751	280	∞	36.3	1.74	623
12.0–12.5	894	330	∞	26.2	1.62	520
12.5–13.0	862	230	∞	18.5	1.58	428

3.4. *Corrections for Completeness*

WDs with low tangential velocities can have the same values of RPM as main-sequence subdwarfs with high tangential velocities, so the two types of stars overlap to some extent in RPM. In order to minimize contamination of the WD sample, a minimum tangential velocity $V_{\rm min}$ is chosen. Candidate WDs with $V_{\rm tan} < V_{\rm min}$ are rejected from the sample, and a correction factor χ, referred to as the discovery fraction by Bahcall & Casertano (1986), is included in the WDLF calculation for the rejected stars. Small values of $V_{\rm min}$ introduce more contamination by subdwarfs, whereas high values reduce the contamination at the expense of reducing the WD sample and making the correction factor χ more uncertain. Values of $V_{\rm min}$ near 25–30 km s^{-1} are optimal for selecting WDs from SDSS data, because contamination is tolerable and χ is still well determined.

A Monte Carlo kinematic model of the disk WD population is used here to calculate χ for each $V_{\rm min}$. The model is described briefly by Liebert et al. (1999) and is similar to models constructed by others (e.g., Wood & Oswalt 1998; Hansen & Liebert 2003; García-Berro et al. 2004). The important input parameters are the values of the velocity ellipsoid for disk WDs in the

TABLE 2
Completeness for Disk WDs with $V_{\rm tan} > V_{\rm min}$

$V_{\rm min}$ (km s^{-1})	χ All Sky	χ SDSS DR3
0	1.000	1.000
5	0.990	0.991
10	0.961	0.965
15	0.914	0.924
20	0.852	0.869
25	0.780	0.802
30	0.700	0.726
35	0.616	0.646
40	0.532	0.565
45	0.452	0.486
50	0.377	0.410
60	0.248	0.276
70	0.154	0.174
80	0.090	0.102
90	0.049	0.056
100	0.026	0.029
110	0.014	0.015
120	0.007	0.007
130	0.004	0.004
140	0.002	0.002

solar neighborhood. Here we use the values of dM stars in the solar neighborhood from Reid et al. (1995): 43, 31, 25, and -22 km s^{-1} for σ_U, σ_V, σ_W, and the lagging rotation velocity relative to the local standard of rest (often called the asymmetric drift), respectively. The resulting values of χ are given in Table 2, in which values are given for the full sky and for the part of the sky included in our SDSS sample. The two values are slightly different because different lines of sight see different projections of the velocity ellipsoid. These values for the velocity ellipsoid are larger than are often cited for the thin disk because the WD population (especially at the low luminosities included in this paper) is older than most constituents of the thin disk, but they are smaller than for the thick disk (e.g., Reid 2005). Experiments with other plausible parameters for the velocity ellipsoid indicate that the uncertainty in χ is about 10% of $(1 - \chi)$. Therefore, the uncertainty has little effect on the derived WDLF, even for $V_{\rm min} = 40$ km s^{-1}.

A second correction is needed for completeness of the USNO-B Catalog and its match with SDSS objects. This correction depends on magnitude, color, and proper motion. Both Monet et al. (2003) and Munn et al. (2004) provide relevant data, but here we apply some restrictions to reduce contamination (see § 3.5), so new completeness values have been calculated. We have run all the stars in DR3 through the same USNO-B matching and selection used for the WD selection, except for the proper motion and tangential velocity limits. We assume that the SDSS catalog of stars is complete and find the completeness of the USNO-B matches. The large numbers of stars provide accurate measures of completeness versus magnitude and color: the completeness varies over 86%–95% for $g < 19.25$, 83%–94% for $g < 19.5$, and 78%–93% for $g < 19.75$, depending on color. The completeness is also a function of proper motion (Gould 2003; Munn et al. 2004), being essentially complete for proper motions less than 40 mas yr^{-1}, dropping to about 70% complete for proper motions of 1000 mas yr^{-1}, in addition to the above magnitude-dependent factor. The correction at small proper motion (less than 100 mas yr^{-1}) was derived by comparison with SDSS data along the celestial equator in the fall sky, which has been observed many times over a period of 5 years and for which SDSS-based proper motions are thus available. For larger proper motions, the correction was derived by comparison with the revised New Luyten Two Tenths Catalog (rNLTT; Salim & Gould 2003), under the assumption that the rNLTT is itself 90% complete (Lépine & Shara 2005). The combined overall completeness for WDs in this sample is near 70%, and the uncertainty is estimated to be of order 10%. The correction (vs. magnitude, color, and proper motion) has been applied.

3.5. *Corrections for Contamination*

Contamination of the WD sample occurs in two ways. First, nondegenerate stars sometimes have a spurious large measured proper motion and thus acquire a large RPM that can scatter the star into the WD sample. Because F, G, and K main-sequence stars are so numerous in the SDSS, even a very small fraction of bad proper motion measurements (usually caused by confusion in matching the five plate detection lists in USNO-B) can cause noticeable contamination. To minimize this source of contamination, we require stars with $g - i > 0.12$ (for which the stellar main sequence becomes heavily populated in the SDSS) to match on *all five* USNO-B plates, as well as to match the SDSS detection within 1″ at the epoch of the SDSS scan and to have no other SDSS source with $g < 22$ within 7″ (see Kilic et al. 2006). For stars with $g - i < 0.12$ (for which potential contaminants are far less numerous), we relax these restrictions and accept objects detected on as few as three USNO-B plates and the SDSS. (However, in § 5 we discuss WDs found to have high tangential velocities. For those rare objects, the relaxed selection allows some contamination, so in § 5 we revert back to the tighter restrictions for high-velocity WDs.) These restrictions were chosen after inspecting many WD candidates (and all cool WD candidates) on digital scans of the sky survey plates used for USNO-B to verify their proper motions.[13]

A second source of contamination is nondegenerate stars with correctly measured proper motions and with very high tangential velocities that give RPM values in the WD selection region. These can be either hot sdO and sdB stars or cooler main-sequence subdwarfs. The choice of $V_{\rm min}$ has a strong effect; $V_{\rm min} = 15$ km s^{-1} allows a significant number of real contaminating stars, whereas $V_{\rm min} = 30$ km s^{-1} eliminates most of them. Only spectra can identify these contaminants; Kilic et al. (2006) show that this contamination is at most a few percent, and probably much less. Using these restrictions, we find contamination of 1%–2% for most of the WD sample, exemplified by four SDSS QSOs that have entered our sample. The LFs below are corrected by these small factors.

3.6. *Cool White Dwarfs with Helium Atmospheres*

Figure 2 shows that for WDs with $g - i > 0.7$, corresponding to temperatures cooler than 5500 K and $M_{\rm bol} > 14.5$, the distance and luminosity of a star with a helium-dominated atmosphere will be underestimated if the pure hydrogen curve is assumed to be correct and is used for the photometric distance determinations described in § 3.2. Spectra generally do not help because, with the exception of a small fraction of stars with carbon or calcium features, most cool WDs with either hydrogen or helium atmospheres have featureless DC spectra. A combination of accurate optical and infrared photometry usually can distinguish their type (Bergeron et al. 2001), but infrared photometry is not currently available for most of our sample. (Only about 5% of the WDs in

[13] Available at http://www.nofs.navy.mil/data/fchpix.

TABLE 3
Adopted Fractions of H- and He-Atmosphere Stars

Initial, If Hydrogen		Revised, If Helium		Best Fractions		Alternative A		Alternative B	
M_{bol}	T_{eff}	M_{bol}	T_{eff}	H	He	H	He	H	He
<15.20	>4650	...	...	1.0	0.0	1.0	0.0	1.0	0.0
15.20–15.50	4330–4650	14.86–15.01	4850–5020	0.5	0.5	0.8	0.2	0.3	0.7
15.50–16.00	3850–4330	15.01–15.19	4650–4850	0.2	0.8	0.5	0.5	0.1	0.9
>16.00	<3850	>15.19	<4650	0.0	1.0	0.2	0.8	0.0	1.0

this sample are detected in the Two Micron All Sky Survey Point Source Catalog. We are in the process of obtaining infrared photometry for many of the cool WDs in the sample.) Therefore, for cool WDs we calculate the distance and luminosity of each star under both hydrogen and helium assumptions and assign a fraction (depending on the color of the star) to each type based on our knowledge of the H/He ratios of cool WDs from the literature. A similar procedure was followed by Knox et al. (1999). Here, however, each star's assignment is neither total hydrogen versus helium nor random; instead, each star can contribute to the WDLF as both types through a weight W.

The fraction of hydrogen and helium atmosphere types that we adopt for cool WDs is based on the following facts: few helium-atmosphere WDs are known with temperatures in the range 5000–6000 K (Bergeron et al. 2001), and only in the cooler half of this temperature range does the composition matter for our purposes; the fraction of known hydrogen-atmosphere WDs is 40%–50% in the temperature range 4000–5000 K (Bergeron et al. 2001); for temperatures below 4000 K, the few known WDs probably have helium-dominated (but not pure helium) atmospheres (Bergeron et al. 2001; Bergeron & Leggett 2002; Gates et al. 2004). Because cool WDs with helium atmospheres are more luminous at a given color (by 0.7 mag at $g - i = 1.3$, for example), they can be seen at greater distances (1.4 times greater, for the same example) than those with hydrogen atmospheres. Therefore, in a magnitude-limited sample such as SDSS, in the reddest color range we should expect to find about 3 times more helium-atmosphere stars, if the two types have equal space densities in that color range.

In order to reach results that are consistent with the above facts, the criteria given in Table 3 are adopted. These criteria include the most likely H/He mix, labeled "best fractions" in Table 3, and two alternative mixes that favor more hydrogen types (alternative A) and more helium types (alternative B). All three mixes are used below to show the sensitivity of our results to the H/He assumptions. Ultimately, a determination of each star's atmospheric composition is needed to help reduce the present ambiguity.

4. WHITE DWARF LUMINOSITY FUNCTION

The LF is derived from the list of identified WDs by summing the inverse volume of space in which each star potentially would have been included within the sample limits, calculating each luminosity bin separately. The derived WDLF is shown in Figure 4. A scale height of 250 pc and a tangential velocity limit of 30 km s^{-1} have been adopted.

The result at the bright end is in acceptable agreement with results from the Palomar-Green (PG) survey. The latest analysis of DA stars only in the PG survey (Liebert et al. 2005) is shown in Figure 4, in which their M_V space densities have been converted to M_{bol} space densities. Accounting for non-DA stars, as was done by Leggett et al. (1998), raises the densities from the PG survey by a small amount. The PG survey gives densities in agreement with SDSS results for $7 < M_{bol} < 10$ but smaller than SDSS by factors of 2–3 for $10 < M_{bol} < 13$ or $11.3 < M_V < 13.2$. This is exactly the range in which Liebert et al. (2005) suspect the PG survey results are incomplete. Both curves are plotted here, assuming a scale height of 250 pc.

The result at the faint end is in excellent agreement with that from the local sample selected from the Luyten half-second (LHS) survey (Leggett et al. 1998). It agrees with two other similar proper motion–selected studies, Boyle (1989) and Knox et al. (1999). It does not agree with some other results that have suggested the LHS sample is incomplete. We return to this point below. The drop in density at the faint end is not yet a secure result, and we also discuss this important issue below. The integral of the curve in Figure 4 gives a space density of WDs in the solar neighborhood of 0.0046 ± 0.0005 pc^{-3}. The assumptions made here about the scale height and the fraction of He-atmosphere stars affect this result, but not drastically (see next paragraphs). The space density is somewhat higher than found by Leggett et al. (1998), 0.0034 pc^{-3}, but lower than found by Holberg et al. (2002), 0.0050 pc^{-3}.

The effect of varying the tangential velocity selection limit V_{lim} is shown in Figure 5. Ideally, the correction factor χ would

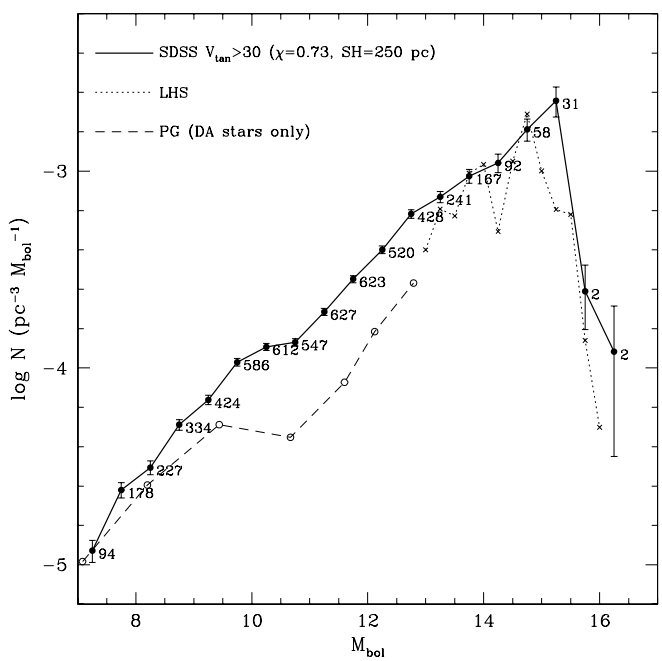

Fig. 4.—LF derived in this paper. The number of stars used for each data point is indicated. Two results from the literature are shown for comparison: the dotted line at the faint end is taken from Leggett et al. (1998), based on the LHS catalog; the dashed line at the bright end is taken from Liebert et al. (2005), based on analysis of the PG survey, including DA WDs only.

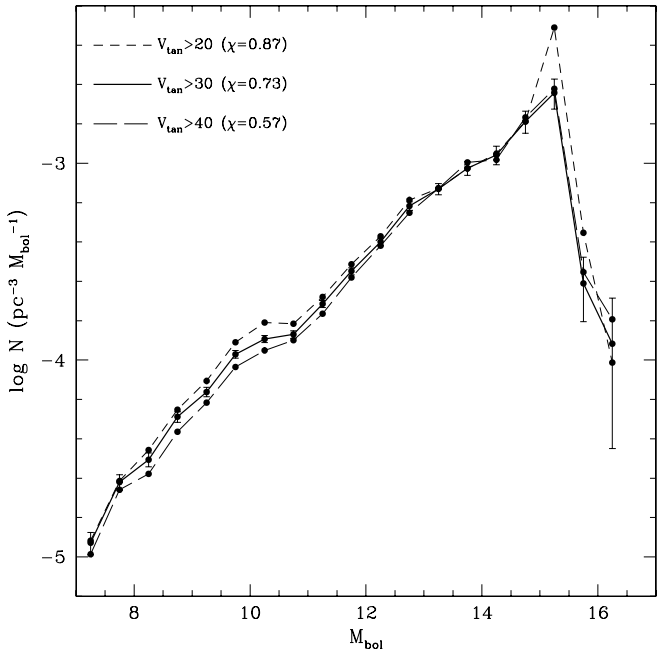

FIG. 5.—LF derived using different lower limits for the tangential velocity. The factor (χ) used to account for low-velocity WDs below the selection limit is described in the text.

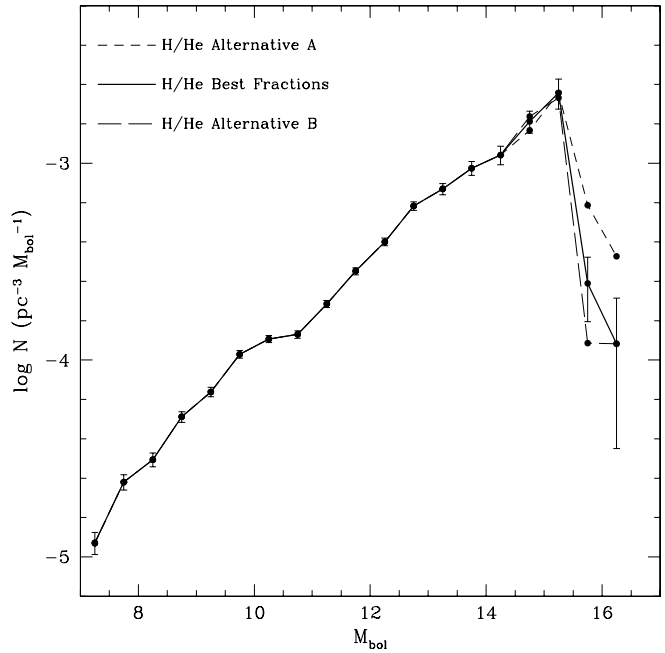

FIG. 7.—LF derived assuming different fractions of hydrogen- and helium-dominated atmospheres for the coolest WDs.

correctly account for stars missed below the limit, and these curves would coincide. The higher densities derived using $V_{\rm lim} = 20$ km s^{-1} suggest that some contamination is entering the sample more than has been accounted for. Contamination is expected to be a factor for the faintest two bins, in which the number of WDs is dropping but the space density of cool subdwarfs is continuing to rise, and they enter the WD sample at bright RPM values when a small $V_{\rm lim}$ value is used.

The effect of using different values for the disk scale height is shown in Figure 6. This factor affects only the bright end of the WDLF. As discussed in §§ 3.3 and 5, a value of 300 pc

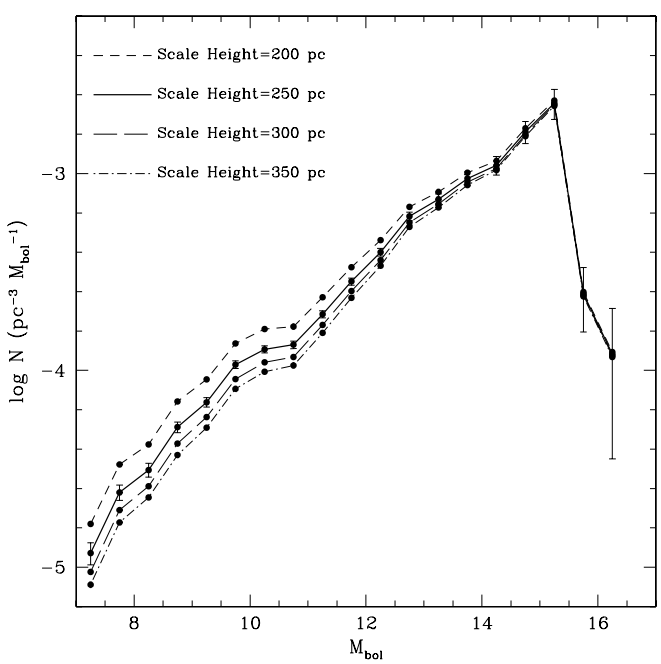

FIG. 6.—LF derived using different values for the scale height of the Galactic disk.

or more is suggested from the SDSS imaging data in this paper. A more accurate analysis should be possible using hotter WDs in the SDSS, either from photometric selection or from spectra, because they reach distances well beyond one scale height.

The different possible mixtures of hydrogen-dominated and helium-dominated atmospheres given in Table 3 result in the different WDLF results shown in Figure 7. As expected, adopting a higher fraction of hydrogen-dominated stars (alternative A) results in more stars being assigned fainter luminosities and gives a less pronounced drop and a more extended faint tail to the LF. There are very few stars in the faintest luminosity bins, and we currently know nothing about the H/He type of each individual star beyond the likely types discussed in § 3.6. Furthermore, lacking a parallax for each star, the possibility of an abnormal mass adds to the uncertainty in any conclusions from these data. Particularly, for the two ultracool stars that are assigned $M_{\rm bol} = 16.2$ (§ 3.2), one has a known luminosity, but the other does not and could well be lower luminosity. Therefore, the present results must be considered preliminary. We can conclude that the SDSS data indicate a rapid decline in the WDLF at $M_{\rm bol} > 15.4$, a result that supports conclusions from the LHS sample. However, the shape of the drop, the exact luminosity of the drop, and the extent of the faint tail are currently better determined from the LHS sample than from the SDSS data.

5. DISCUSSION

The WDLF derived here and shown in Figure 4 is remarkably smooth and featureless. The only noticeable feature in the range $8 < M_{\rm bol} < 15$ is the small plateau near $M_{\rm bol} = 10.5$. A plot with finer binning is shown in Figure 8. There it is seen that the feature is actually a flattening at $M_{\rm bol} = 10.0-10.5$ and a drop at $M_{\rm bol} = 10.7$, corresponding to a temperature boundary of 13,200 K ($g - i = -0.45$) for DA stars. The ZZ Ceti instability strip is at slightly cooler temperatures, also shown in the figure, so it is probably not related to this feature. There is no significant contamination of the sample by nondegenerate stars or

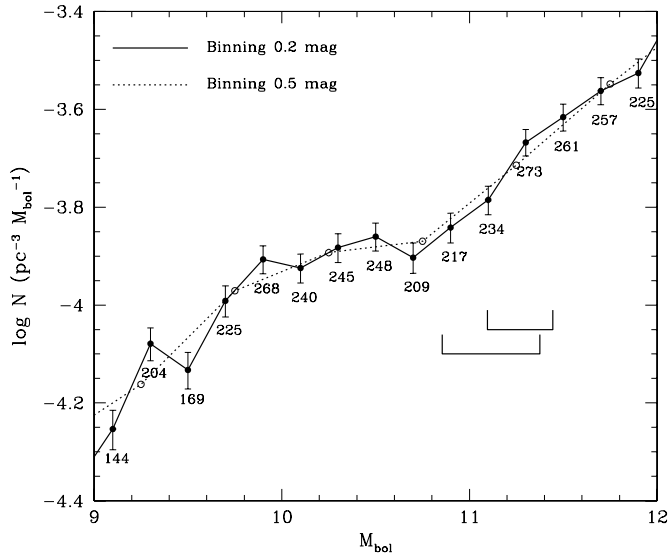

FIG. 8.—Higher resolution plot of the middle portion of Fig. 4. The two bars below the curve near $M_{\rm bol} = 11$ show the location of the ZZ Ceti instability strip observed by Mukadam et al. (2004; *top*) and Bergeron et al. (2004; *bottom*).

QSOs near this color. The feature could be an artifact caused by incorrect models of stars near this temperature, which could in turn cause incorrect photometric distances and/or incorrect values of $M_{\rm bol}$ to be assigned. However, the models are believed to be quite accurate in this temperature range. No feature is predicted (Fontaine et al. 2001) from a pause in WD cooling and dimming. If the feature is real, it could reflect a nonuniform rate of production of WDs in the Galactic disk. Noh & Scalo (1990) modeled the effect that bursts of star formation would have on the WDLF and suggested that a tentative bump seen in the WDLF (Liebert et al. 1988) might be caused by such a burst 0.3 Gyr ago. The cooling time for a normal-mass WD to reach $M_{\rm bol} \sim 10.5$ is 0.3 Gyr, and the main-sequence lifetime of a likely progenitor is ~2.5 Gyr, suggesting that a drop in star formation about 3 Gyr ago (after a burst or a long-duration higher rate of star formation) might be the cause of the plateau seen here in Figure 8. Further models like those of Noh & Scalo would help quantify this suggestion.

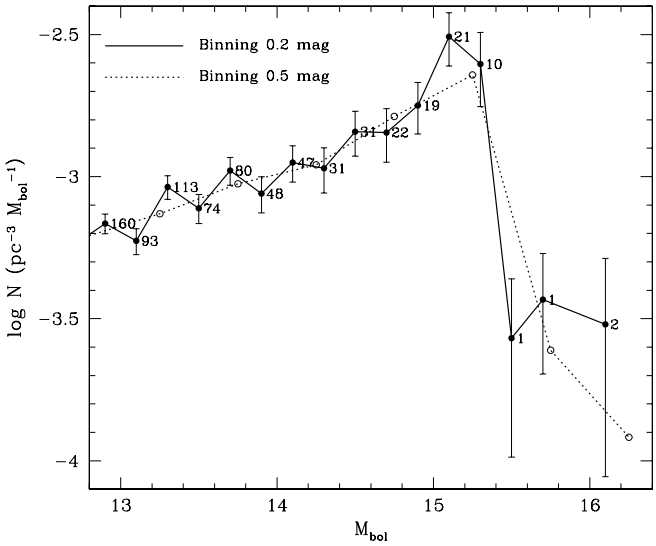

FIG. 9.—Higher resolution plot of the low-luminosity end of Fig. 4.

TABLE 4

COMPLETENESS FOR HALO WDS WITH $V_{\rm tan} > V_{\rm min}$

$V_{\rm min}$ (km s^{-1})	χ All Sky	χ SDSS DR3
0	1.000	1.000
100	0.854	0.893
120	0.792	0.842
140	0.724	0.782
160	0.648	0.712
180	0.568	0.633
200	0.488	0.551
220	0.409	0.465
240	0.333	0.383
260	0.265	0.307
280	0.206	0.240
300	0.155	0.183

The cool end of the WDLF from Figure 4 is shown with finer binning in Figure 9. (The sawtooth shape in Fig. 9 is apparently a statistical fluke, as we have checked for errors introduced by improper binning.) The abrupt drop in the LF occurs at $M_{\rm bol} = 15.40$, although the exact shape of the drop and the exact luminosity at which it occurs both depend on the unknown H/He type of WDs in this sample, as discussed above. Also evident in this plot is a rise in the LF at $M_{\rm bol} = 15.1-15.2$. This rise appears to be marginally significant. It is at a luminosity consistent with the predicted onset of convective coupling between the convective hydrogen atmosphere and the degenerate core (Fontaine et al. 2001), causing temporary additional release of internal energy and delayed cooling. Observationally, the rise in Figure 9, like the following drop, is sensitive to the assumptions made here about H/He types and about the luminosity of the coolest stars. Further study of these stars should help to verify the reality and exact shape of this feature.

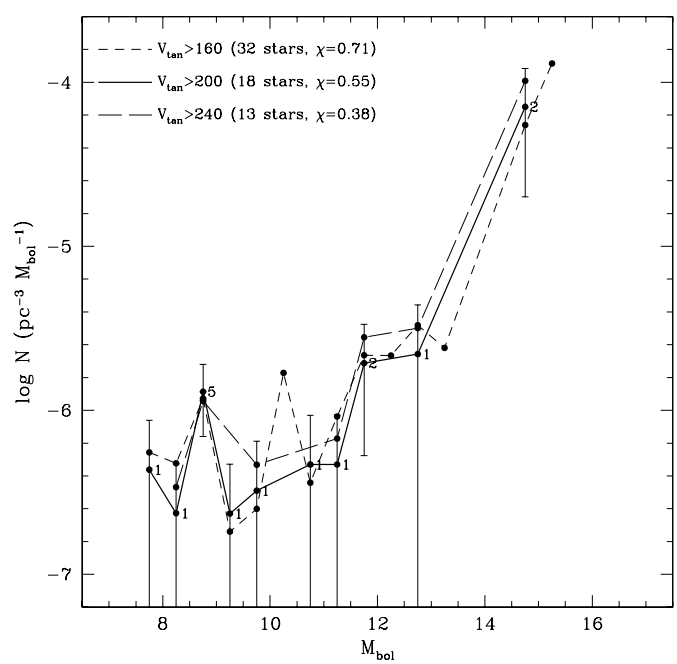

FIG. 10.—Preliminary LF for high-velocity WDs. The three curves show the LF using different selection limits of tangential velocity and after correction for incompleteness using the listed values of χ. The sample may be dominated by halo WDs but probably includes some fractions of disk, thick-disk, and high-mass WDs (see text).

TABLE 5
WDs with Possible High Tangential Velocities

R.A. (deg)	Decl. (deg)	g	$g-i$	$M_{\rm bol}$	D (pc)	$\mu_{\rm R.A.}$ (mas yr^{-1})	$\mu_{\rm decl.}$ (mas yr^{-1})	$V_{\rm tan}$ (km s^{-1})	Spectral Type	Notes
15.5302	−0.5499	18.18	−0.20	11.64	163	344	−126	282	DA	1
45.8551	−8.1430	18.74	−0.33	10.50	256	191	49	239	DA	2
125.9965	31.1984	18.12	−0.64	8.65	310	−16	−164	242	DA	
134.6315	42.4896	18.53	0.05	12.74	124	−229	−203	180	DA	3
139.3937	2.1568	18.87	−0.54	8.72	430	−98	−41	216	DA	2
140.1324	2.9664	18.55	−0.34	11.11	230	−74	−219	252		
151.1846	8.6299	18.06	−0.66	8.57	308	−173	−59	267	DA	
152.3864	52.7773	18.59	−0.48	10.21	286	−56	−114	172	DA	
156.3491	0.7183	18.44	0.73	14.54	47	−63	−1114	248	DA	4
158.8389	61.1174	18.45	−0.62	8.56	377	−40	−113	214	DA	
159.9244	46.2068	18.81	−0.05	12.43	159	−224	−132	196	DZ	5
161.4964	59.0801	17.76	0.05	12.70	88	−1022	−1464	746	DQ	6
166.8808	48.9231	19.47	1.25	15.09	49	−726	−79	171	DC	7, 8
170.0118	44.4748	18.56	−0.44	10.48	265	−90	−99	168		
172.8554	9.2366	18.83	−0.64	8.30	449	−69	33	163		
181.8450	9.2898	19.41	−0.24	11.60	294	114	−260	395		
184.3810	61.0892	18.06	−0.83	6.20	534	−76	−66	255	DA	
190.1810	67.1766	18.25	−0.63	8.44	346	−183	−92	336		
193.7839	46.9218	19.19	1.14	14.97	49	−1089	−114	252		8
193.7839	46.9218	19.19	1.14	15.40	38	−1089	−114	197		9
194.4960	−2.2204	19.15	−0.72	7.69	621	−71	−24	220	DB	2
195.5034	1.7721	18.31	−0.47	10.37	240	−140	−50	169		
206.4670	40.0171	18.59	−0.63	8.66	396	−194	−54	378	DA	
216.7079	9.8268	17.89	−0.55	9.69	228	47	−321	351		10
222.2287	5.3177	18.00	−0.58	8.64	287	−132	−16	181		
223.1366	10.8904	18.74	−0.72	7.74	504	−58	−35	162		
225.6319	1.1794	18.46	0.39	11.82	174	−79	−195	174	DA + M	2, 11
240.3110	53.7709	18.49	0.14	13.08	104	74	−385	194	DA	2
243.6112	38.5146	19.22	−0.96	2.38	1484	14	−41	305		
245.7565	30.5115	17.91	−0.61	9.14	261	3	−162	201		
332.9242	11.6012	19.27	−0.13	12.00	229	58	−165	190		
342.5009	12.6722	19.50	−0.25	11.27	316	130	−16	196	DQ	
355.2922	0.5499	19.14	−0.46	10.39	343	9	−106	173	DA	2

Notes.—(1) LP 586-51; in Oppenheimer et al. (2001); (2) in Kleinman et al. (2004); (3) LP 210-12; (4) LHS 282; (5) LP 168-8; (6) LHS 291; (7) in Lépine et al. (2003); (8) D assuming helium atmosphere; (9) D assuming hydrogen atmosphere; (10) LP 500-28; (11) LP 621-58.

The analysis in this paper has assumed that the WD population has a distribution away from the Galactic plane that can be described with a single exponential scale height. The WD population is actually more complicated because the mean age of hot, luminous WDs is systematically younger than that of cool, low-luminosity WDs.[14] Stars in the Galactic disk have been perturbed over time, so old populations have higher velocity dispersions and larger scale heights (e.g., Wielen 1977; Dehnen & Binney 1998). How much does this disk heating affect the present analysis? Over the range of WD luminosities included in this paper, their properties change as follows: $M_{\rm bol}$ changes from 8 to 13 to 15; the WD mass drops from 0.63 to 0.59 to 0.58 $M_\odot$, and the WD cooling age increases from 0.04 to 1.2 to 6.2 Gyr (Bergeron et al. 1995); the initial progenitor mass drops from 1.9 to 1.5 to 1.4 $M_\odot$ (Ferrario et al. 2005); the main-sequence lifetime increases from 2 to 3 to 4 Gyr; the total age increases from 2 to 4 to 10 Gyr; the vertical velocity dispersion σ_W increases from 12 to 18 to 27 km s^{-1} (Nordström et al. 2004); and the scale height increases from 250 to 350 to roughly 500 pc (Mihalas & Binney 1981). At the low-luminosity end of the range discussed here, the increased velocity dispersion causes greater completeness of the sample (a higher value of χ), and the increased scale height also causes greater completeness by a tiny amount shown in Figure 6. The two factors would act to reduce the derived WDLF slightly were we to include them in the analysis. The changing scale height with WD luminosity has a bigger influence on the total surface density of WDs in the Galactic disk, however. This factor will be important when interpreting the WDLF to derive the star formation history of the disk.

A small fraction of WDs have large values of H_g and, if they are normal WDs, high tangential velocities. The analysis described above gives 80 stars with $V_{\rm tan} > 160$ km s^{-1}, about 1% of the total WD population found here. A few are WDs but with spurious proper motions; applying a more restrictive selection (requiring detection on all five plates in USNO-B and excluding stars with another star nearby for all stars, not just redder stars; see § 3.5) gives 32 stars with $V_{\rm tan} > 160$ km s^{-1} (0.6% of the total). Table 2 shows that a population with disk kinematics is expected to have less than 0.1% with tangential velocities this

[14] The WD population is further complicated because a one-component Gaussian velocity ellipsoid and a single scale height are not realistic at *any* luminosity. For example, both Hansen & Liebert (2003) and Reid (2005) suggest reference models for thin-disk WDs that have smaller values for the velocity dispersion and scale height than are adopted here. However, both papers discuss the excess of high-velocity WDs that are observed. Understanding their origin in the thin or the thick disk (Bergeron et al. 2005; Reid 2005) will require much more work.

high.[15] The excess found here can come from halo stars, thick-disk stars (e.g., Reid 2005), or thin-disk "runaway" stars with anomalously high velocities (e.g., Bergeron et al. 2005). It can also come from thin-disk stars that have high mass and therefore erroneously high derived values of luminosity, distance, and $V_{\rm tan}$; LHS 4033, from the Oppenheimer et al. (2001) sample, is an example of such a high-mass WD (Dahn et al. 2004). Further data about these high-velocity candidates come from SDSS spectra of 34 stars: 11 are non-DA WDs, mostly DB or DQ, so they are still candidates for high-velocity stars, but we have little information about their masses and exact luminosities; 23 are DA WDs, and determination of their gravities by fitting the hydrogen line profiles in their spectra with the procedure in Kleinman et al. (2004) shows that 21 have normal values of $\log g \sim 8.0$ and only two have $\log g > 8.5$ and are probably high-mass stars. These spectra indicate that only a few of the 80 high-velocity candidates are actually high-mass stars instead.

If we make the assumption that all the high-velocity candidates are halo stars, we can construct a LF. To account for the halo stars with $V_{\rm tan}$ below the adopted cutoff, χ-corrections must be applied; Table 4 gives these values, calculated in the same way as described in § 3.4 and based on the halo velocity ellipsoid from Morrison et al. (1990). Figure 10 shows the LF using the restrictive sample of 32 high-velocity WDs for three different $V_{\rm tan}$ cutoffs. Table 5 gives this high-velocity sample. The fact that the LF derived using the higher cutoffs does not drop much suggests that the sample is not dominated by a rapidly dropping high-velocity tail of the thick disk or the thin disk. However, the sample can have significant numbers of "runaway" WDs from the thin disk or thick disk that have somehow acquired a velocity kick, and therefore do not follow the velocity distributions assumed in the models. Therefore, the LF in Figure 10 should be considered as an upper limit for the halo until the actual composition of the sample is better understood. The shape of the LF (rising toward lower luminosities) and the integrated space density (4×10^{-5} pc^{-3}) are both consistent with models of an old, single-burst population (e.g., Hansen 2001); they are probably consistent with an interpretation of the Oppenheimer (2001) sample in which some allowance is made for contamination by disk stars (e.g., Torres et al. 2002). However, the halo/thick-disk/thin-disk composition of this sample must be better understood before using it to derive a space density for halo WDs.

[15] Note that a $V_{\rm tan}$ limit at a velocity lower than 140 km s^{-1} is expected to include significant numbers of thin-disk WDs, according to Table 2, based on the velocity ellipsoid used in § 3.4. Contamination by the thick-disk WDs is expected to be even greater with a low velocity limit (Reid 2005).

J. L. and K. A. W. acknowledge support from the National Science Foundation through grant AST 03-07321. This research has made use of the USNOFS Image and Catalogue Archive operated by the United States Naval Observatory, Flagstaff Station (http://www.nofs.navy.mil/data/fchpix). Funding for the creation and distribution of the SDSS Archive has been provided by the Alfred P. Sloan Foundation, the Participating Institutions, the National Aeronautics and Space Administration, the National Science Foundation, the US Department of Energy, the Japanese Monbukagakusho, and the Max Planck Society. The SDSS Web site is at http://www.sdss.org.

The SDSS is managed by the Astrophysical Research Consortium for the Participating Institutions. The Participating Institutions are the University of Chicago, Fermilab, the Institute for Advanced Study, the Japan Participation Group, the Johns Hopkins University, the Korean Scientist Group, Los Alamos National Laboratory, the Max Planck Institute for Astronomy, the Max Planck Institute for Astrophysics, New Mexico State University, the University of Pittsburgh, Princeton University, the United States Naval Observatory, and the University of Washington.

REFERENCES

Abazajian, K., et al. 2004, AJ, 128, 502
———. 2005, AJ, 129, 1755
Bahcall, J. N., & Casertano, S. 1986, ApJ, 308, 347
Bergeron, P., Fontaine, G., Billères, M., Boudreault, S., & Green, E. M. 2004, ApJ, 600, 404
Bergeron, P., & Leggett, S. K. 2002, ApJ, 580, 1070
Bergeron, P., Leggett, S. K., & Ruiz, M. T. 2001, ApJS, 133, 413
Bergeron, P., Ruiz, M. T., Hamuy, M., Leggett, S. K., Currie, M. J., Lajoie, C.-P., & Dufour, P. 2005, ApJ, 625, 838
Bergeron, P., Saffer, R. A., & Liebert, J. 1992, ApJ, 394, 228
Bergeron, P., Wesemael, F., & Beauchamp, A. 1995, PASP, 107, 1047
Boyle, B. J. 1989, MNRAS, 240, 533
Dahn, C. C., Bergeron, P., Liebert, J., Harris, H. C., Canzian, B., Leggett, S. K., & Boudreault, S. 2004, ApJ, 605, 400
Dehnen, W., & Binney, J. J. 1998, MNRAS, 298, 387
Digby, A. P., Hambly, N. C., Cooke, J. A., Reid, I. N., & Cannon, R. D. 2003, MNRAS, 344, 583
Downes, R. A. 1986, ApJS, 61, 569
Evans, D. W. 1992, MNRAS, 255, 521
Ferrario, L., Wickramasinghe, D., Liebert, J., & Williams, K. A. 2005, MNRAS, 361, 1131
Fleming, T. A., Liebert, J., & Green, R. F. 1986, ApJ, 308, 176
Fontaine, G., Brassard, P., & Bergeron, P. 2001, PASP, 113, 409
Fukugita, M., Ichikawa, T., Gunn, J. E., Doi, M., Shimasaku, K., & Schneider, D. P. 1996, AJ, 111, 1748
García-Berro, E., Torres, S., Isern, J., & Berkert, A. 2004, A&A, 418, 53
Gates, E., et al. 2004, ApJ, 612, L129
Gould, A. 2003, AJ, 126, 472
Green, R. F. 1980, ApJ, 238, 685
Gunn, J. E., et al. 1998, AJ, 116, 3040
Hansen, B. M. S. 2001, ApJ, 558, L39
Hansen, B. M. S., & Liebert, J. 2003, ARA&A, 41, 465
Harris, H. C., Dahn, C. C., Vrba, F. J., Henden, A. A., Liebert, J., Schmidt, G. D., & Reid, I. N. 1999, ApJ, 524, 1000
Harris, H. C., et al. 2001, ApJ, 549, L109
———. 2003, AJ, 126, 1023
Hogg, D. W., Finkbeiner, D. P., Schlegel, D. J., & Gunn, J. E. 2001, AJ, 122, 2129
Holberg, J. B., Oswalt, T. D., & Sion, E. M. 2002, ApJ, 571, 512
Ishida, K., Mikami, T., Noguchi, T., & Machara, H. 1982, PASJ, 34, 381
Ivezić, Z., et al. 2004, Astron. Nachr., 325, 583
Kilic, M., von Hippel, T., Munn, J. A., Harris, H. C., Liebert, J., Metcalfe, T. S., Williams, K. A., & Winget, D. E. 2006, AJ, 131, 582
Kilic, M., Winget, D. E., von Hippel, T., & Claver, C. F. 2004, AJ, 128, 1825
Kleinman, S. J., et al. 2004, ApJ, 607, 426
Knox, R. A., Hawkins, M. R. S., & Hambly, N. C. 1999, MNRAS, 306, 736
Leggett, S. K., Ruiz, M. T., & Bergeron, P. 1998, ApJ, 497, 294
Lépine, S., & Shara, M. M. 2005, AJ, 129, 1483
Lépine, S., Shara, M. M., & Rich, R. M. 2003, AJ, 126, 921
Liebert, J., Bergeron, P., & Holberg, J. B. 2005, ApJS, 156, 47
Liebert, J., Dahn, C. C., Harris, H. C., & Leggett, S. K. 1999, in ASP Conf. Ser. 169, 11th European Workshop on White Dwarfs, ed. J.-E. Solheim & E. G. Meistas (San Francisco: ASP), 51
Liebert, J., Dahn, C. C., & Monet, D. G. 1988, ApJ, 332, 891
Lupton, R., Gunn, J. E., Ivezić, Z., Knapp, G. R., Kent, S., & Yasuda, N. 2001, in ASP Conf. Ser. 238, Astronomical Data Analysis Software and Systems X, ed. F. R. Hamden, F. A. Primini, & H. E. Payne (San Francisco: ASP), 269
Mihalas, D., & Binney, J. 1981, Galactic Astronomy (San Francisco: Freeman)
Monet, D. G., et al. 2003, AJ, 125, 984
Morrison, H. L., Flynn, C., & Freeman, K. C. 1990, AJ, 100, 1191
Mukadam, A. S., Winget, D. E., von Hippel, T., Montgomery, M. H., Kepler, S. O., & Costa, A. F. M. 2004, ApJ, 612, 1052
Munn, J. A., et al. 2004, AJ, 127, 3034

Nelson, C. A., Cook, K. H., Axelrod, T. S., Mould, J. R., & Alcock, C. 2002, ApJ, 573, 644
Noh, H.-R., & Scalo, J. 1990, ApJ, 352, 605
Nordström, B., et al. 2004, A&A, 418, 989
Oppenheimer, B. R., Hambly, N. C., Digby, A. P., Hodgkin, S. T., & Saumon, D. 2001, Science, 292, 698
Oswalt, T. D., Smith, J. A., Wood, M. A., & Hintzen, P. 1996, Nature, 382, 692
Pier, J. R., Munn, J. A., Hindsley, R. B., Hennessy, G. S., Kent, S. M., Lupton, R. H., & Ivezić, Z. 2003, AJ, 125, 1559
Raymond, S. N., et al. 2003, AJ, 125, 2621
Reid, I. N. 2005, ARA&A, 43, 247
Reid, I. N., Hawley, S. L., & Gizis, J. E. 1995, AJ, 110, 1838
Salim, S., & Gould, A. 2003, ApJ, 582, 1011
Schlegel, D. J., Finkbeiner, D. P., & Davis, M. 1998, ApJ, 500, 525
Smith, J. A., et al. 2002, AJ, 123, 2121
Smolcić, V., et al. 2004, ApJ, 615, L141
Stoughton, C., et al. 2002, AJ, 123, 485
Torres, S., García-Berro, E., Burkert, A., & Isern, J. 2002, MNRAS, 336, 971
Vennes, S., Smith, R. J., Boyle, B. J., Croom, S. M., Kawka, A., Shanks, T., Miller, L., & Loaring, N. 2002, MNRAS, 335, 673
Wielen, R. 1977, A&A, 60, 263
Wood, M. A., & Oswalt, T. D. 1998, ApJ, 497, 870
York, D. G., et al. 2000, AJ, 120, 1579